18th Australasian Fluid Mechanics Conference

Launceston, Australia

3-7 December 2012

Turbulence Modification in Shear Thinning Fluids: Preliminary Results for Power Law Rheology

M. Rudman and H.M. Blackburn

Department of Mechanical and Aerospace Engineering

Monash University, Victoria 3800, Australia

Abstract

Direct numerical simulations of the turbulent pipe flow of power-law fluids are analysed in order to understand the way in which shear thinning affects turbulence. For a generalised Reynolds number of 7500, as the fluid becomes more shear thinning, the log-layer mean velocity profile deviates further above the Newtonian case. Second-order turbulence statistics show a decrease for all correlations except for the axial turbulence intensity which increases marginally over its Newtonian counterpart. The results show that the turbulent kinetic energy budget is modified by new terms that arise in the energy equation.

Introduction

Flows of non-Newtonian fluids occur in a wide range of practical applications including fine-particle mineral suspensions, sewage sludges, molten polymers, bodily fluids, paints and food products such as molten chocolate and mayonnaise. A range of different types of non-Newtonian fluids exist but they can be broadly categorised as being either visco-elastic or not. Turbulent drag reduction in visco-elastic flows has been of particular interest and has resulted in numerous studies (e.g. [1], [5]). In other practical applications (e.g. minerals suspensions, sewage sludges) visco-elasticity is not relevant. For low to moderate concentration suspensions such as those found in minerals tailings applications, shear rheology alone is usually sufficient to describe the suspensions [6]. These fluids are well categorised with a non-uniform viscosity that can depend on the local properties of the flow as well as the time history of the material.

When history effects are not important and the viscosity can be approximated as a local function of the instantaneous velocity field, the fluid is known as a Generalised Newtonian (GN) fluid. In this paper we consider GN fluids in which the dynamic viscosity η is a function of the second invariant of the rate-of-strain tensor $\dot{\gamma}$, *i.e.*

$$\eta=\eta(\dot{\gamma}), \qquad \dot{\gamma}=\sqrt{2s_{ij}s_{ij}}, \qquad s_{ij}=\tfrac{1}{2}\,(\partial u_i/\partial x_j+\partial u_j/\partial x_i) \qquad (1)$$

In many important applications of GN fluids, the effective viscosity (i.e. shear stress divided by shear rate) is very high, and industrially relevant flows can be laminar, e.g. the discharge of thickened slurry in bauxite residue disposal [6]. However, in other cases the volumetric flow rates are sufficiently high or the effective viscosities sufficiently low that the flow can be transitional or turbulent.

Experimental studies of GN fluids in pipe flows date back to the 1950's and 60's e.g. [2], [3]. In [3], the pressure gradient versus bulk velocity was measured for a range of fluids that were nominally well-modelled with a power law rheology i.e.

$$\eta=K\dot{\gamma}^{n-1} \qquad (2)$$

where K is the consistency and n is the flow index. Here, $0 < n < 1$ is known as a shear thinning fluid and $n > 1$ a shear-thickening fluid. It was found that the friction factor expressed as a function of a modified (termed the Metzner–Reed) Reynolds number decreased with decreasing n. A peripheral result to come out of this work is that some low concentration polymeric solutions that appear to behave as GN fluids in laminar flow, display visco-elastic behaviour when the flow becomes transitional or turbulent. This is because the higher shear rates imply smaller time scales which can place the flow in a regime where visco-elastic effects cannot be ignored. Consequently, there is a very real possibility of obtaining good agreement between measurement and simulation for laminar flow of any dilute polymer solution, yet diverging results in the transitional and turbulent flow regime. Consequently, modelling opaque fine particle suspensions with optically clear polymer gels cannot be confidently undertaken solely on the basis of laminar measurements of shear rheology. In addition, unambiguous determination of the effects of modifying rheological parameters is difficult to accomplish in experiments because in practice, different parameters can rarely be varied independently.

Computational modelling of non-Newtonian flows, especially using DNS, shows significant promise in helping to understand transition and turbulence in GN fluids. The main benefit of using a DNS technique is that once validated, it can be reliably used to model the flow behaviour and provide a detailed picture of turbulent structure that is almost impossible to obtain in opaque, fine particle suspensions. DNS has the added benefit that rheological effects such as visco-elasticity can be excluded from the modelling and that the affect of modifying individual rheological parameters can be easily isolated in a simulation. Finally, the technique also allows the validity of rheological models to be assessed in different flow scenarios.

Previous results of DNS of turbulence in GN fluids were presented in [9], [10]. They showed that the effects of shear thinning behaviour on turbulent pipe flow shares similarities with drag reduction in visco-elastic fluids. In agreement with experiment, axial and radial turbulence intensities are reduced in shear-thinning GN fluids whereas axial intensities may increase marginally compared to the Newtonian case. Transition to turbulence, based on a generalised Reynolds number, was also delayed as the shear thinning behaviour increased.

In the present study, the same DNS technique is used to investigate the turbulent pipe flow of power-law fluids for $Re_D \cong 7500$. This extends the Reynolds number range used in [9] and provides a consistent set of results for flow indices spanning from strongly shear thinning (n = 0.4) to shear thickening (n = 1.4). The turbulent kinetic energy budget is calculated for these flows for the first time.

Computational details

Numerical method

We use a spectral element–Fourier discretization that utilizes spectral elements to cover the pipe cross-section and periodic Fourier expansions in the direction of the pipe-axis. The flow is driven with a body force per unit mass in the axial direction that is set to achieve desired flow rates. Execution is fully parallel over planar Fourier modes, product terms are computed pseudo-spectrally and not de-aliased. Time integration is second-order, using backwards-differencing for approximation of temporal derivatives in the velocity-correction scheme. See [10] for details of the method.

Mesh Design

Mesh design is based on a combination of 1) published Newtonian results, 2) our previous experience and 3) a preliminary set of simulations over a range of n=0.4–1.4. We use a single element layout and fixed number of Fourier modes in the streamwise direction, but have varied the spectral element polynomial order, N_p, and domain length to provide an acceptable trade off between resolution and domain size for different rheology. Here we use wall coordinates defined in the usual way except with the constant Newtonian viscosity replaced by the mean wall viscosity given by $\eta_w = K^{1/n}\tau_W^{1-1/n}$ where $\tau_w = \frac{1}{4}D\partial P/\partial z$.

Figure 1 shows the upper part of the 161-element cross-sectional mesh, with details illustrated for polynomial order $N_p = 10$ on the right side of the figure. The first layer of elements is of thickness $\Delta y^+ \approx 9.7$ in the wall-normal direction, the second layer reaches to $\Delta y^+ \approx 26.7$, and on average the third to $\Delta y^+ \approx 51.7$. For $N_p = 10$, the average wall-normal mesh spacing in the first layer of elements is thus $\Delta y^+ \approx 1$, while in the azimuthal direction we have $\Delta x^+ \approx 5.5$. These spacings correspond well to typical values needed for wall-resolving DNS [8].

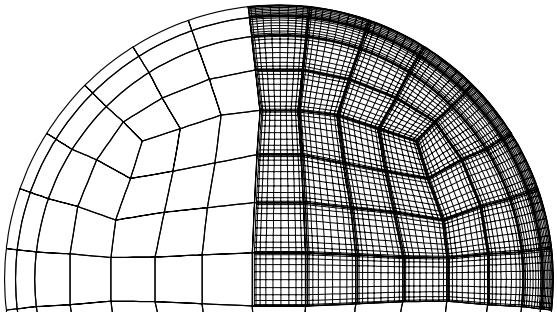

Figure 1 Detail of the upper part of the computational mesh used in the simulations. The left side highlights the spectral elements, and the right side the underlying nodal points for N_p=10.

Element sizes near the centre of the mesh are smaller than required to for Newtonian flow (at Re=7500), however we need better resolution near the centre in GN cases with $n > 1$.

The choice of domain length and streamwise resolution is determined by a need to resolve near-wall structures, and to ensure that the domain lengths are sufficiently long that the periodic boundary condition does not adversely affect the predictions. A streamwise length of L_z = 5D was found in [4] to be sufficient to reduce periodic correlation effects to acceptable levels in a turbulent Newtonian flow DNS. Here, the flow at n=0.4 is transitional, and our preliminary study suggested a domain length of $4\pi D \approx 12.5D$ is required when n=0.4 to contain at least two transitional spots. Thus $L_z = 4\pi$D was chosen as the upper limit of domain length. As the flow index increases, near-wall length scales reduce, (see Figure 2). We adjust the domain length to ensure a minimum value of $2\pi D$ at n=1.4.

In the Newtonian case, we use $L_z = 7.57D$, and mesh spacing in the axial direction of $\Delta z^+ = 11.5$, well below the required value of 15 given in [8]. For the non-Newtonian cases Δz^+ remains approximately constant relative to near-wall length scales because the domain length L_z is adjusted as we change n. Since the near-wall length scales vary in all directions, we also increase the polynomial order at higher n. For $n < 1$ we use $N_p = 10$, (giving approximately 16K mesh points over a 2D pipe cross-section, and 5M nodes in total). For n=1.2 we use N_p=12 (23K 2D nodes and 7.5M nodes in total), and for n=1.4, we use N_p = 14, (giving 32K 2D nodes and 10M total nodes).

Time averaging

Initial conditions are taken from earlier simulations on different meshes or from simulations at different flow indices. Simulations are run until the predicted total wall shear stress approaches the value predicted from the imposed forcing and the superficial flow velocity (U_b) has reaced an almost uniform value. Often both the wall shear stress and superficial velocity will oscillate about a mean value. The integration interval required to reach this state (provided the initial statistical condition is not too far removed from the final condition) is approximately between ten to twenty domain wash-through times. Once steady-state is reached, time-averaged statistics are amassed over another twenty to forty wash-through timescales.

Turbulent Kinetic Energy Budget

To develop energy budgets, we use the Reynolds decomposition with notation $a = A + a'$ to separate a variable into an ensemble-mean and a fluctutating component. Noting that the density is constant, we use the kinematic viscosity $\nu = \eta/\rho$, which is decomposed as $\nu = N + \nu'$. The kinetic energy per unit mass is defined as $E = \frac{1}{2}u_i u_i$ and is also decomposed, $E = Q + q$. The mean flow kinetic energy per unit mass is $Q = \frac{1}{2}U_i U_i$ and the turbulent kinetic energy per unit mass is $q = \frac{1}{2}\overline{u_i' u'}$.

The mean flow energy equation is

$$U_j\frac{\partial Q}{\partial x_j} = -\rho^{-1}\frac{\partial P U_j}{\partial x_j} + 2\frac{\partial N S_{ij}U_i}{\partial x_j} + 2\frac{\partial U_i\overline{\nu' s_{ij}'}}{\partial x_j} - \frac{\partial U_i\overline{u_i' u_j'}}{\partial x_j} - 2N S_{ij}S_{ij} - 2\overline{\nu' s_{ij}'}S_{ij} + \overline{u_i' u_j'}S_{ij}, \tag{3}$$

An equation for the ensemble-average turbulent kinetic energy can be derived and is written

$$\overbrace{U_j\frac{\partial q}{\partial x_j}}^{1} = \overbrace{-\frac{\partial \overline{u_i' u_i' u_j'}}{\partial x_j}}^{2} \overbrace{-\rho^{-1}\frac{\partial \overline{p' u_j'}}{\partial x_j}}^{3} \overbrace{+2\frac{\partial N\overline{s_{ij}' u_i'}}{\partial x_j}}^{4} \overbrace{+2\frac{\partial \overline{\nu' u_i'}S_{ij}}{\partial x_j}}^{5} \overbrace{+2\frac{\partial \overline{\nu' s_{ij}' u_i'}}{\partial x_j}}^{6} \underbrace{-2N\overline{s_{ij}' s_{ij}'}}_{7} \underbrace{-2\overline{\nu' s_{ij}'}S_{ij}}_{8} \underbrace{-2\overline{\nu' s_{ij}' s_{ij}'}}_{9} \underbrace{-\overline{u_i' u_j'}S_{ij}}_{10}. \tag{4}$$

For Newtonian fluids, the numbered terms are usually known as:

1: mean flow advection (MA);
2: turbulent transport (TT);
3: pressure-gradient work (PW);
4: mean viscous transport (MVT);
7: mean viscosity dissipation (MVD);
10: production (PR).

Terms 5, 6, 8 and 9 in equation 4 are zero for a Newtonian fluid, and for a GN fluid are named here:

5: mean shear turbulent viscous transport (MSVT);
6: turbulent viscous transport (TVT);
8: turbulent shear stress–mean strain contraction (TSMS);
9: turbulent viscosity dissipation (TVD).

For pipe flow with constant bulk velocity, the mean flow advection (term 1) is zero. The mean viscosity dissipation (term 7, MVD) is negative-definite, and the corresponding turbulent viscosity dissipation (term 9, TVD) can take either sign because the fluctuating viscosity is not positive definite (and thus it is not strictly a dissipation). Note that the turbulent stress–mean shear contraction (term 8, TSMS) appears with the same sign in both the mean and fluctuating-flow energy equations. Pinho [7] also derives similar equations.

Results

Newtonian results and validation

Validation of the code for these type of flows at lower *Re* is reported in [9]. In addition, data for turbulent flow of Newtonian fluid in a pipe at a nominal bulk flow Reynolds number Re_D = 7500 were compared to the experimental results in [11] for bulk flow Reynolds numbers of 5000 and 10 000 (not shown). The experimental values for mean and fluctuating velocities, Reynolds shear stress and turbulent energy production bracket our simulations results except very close to the wall, where some of the experimental results are acknowledged to be unreliable.

Results for power law fluids

Contours of axial flow velocity at $y^+ \approx 10$ are presented in Figure 2, where black is low speed and white high speed fluid. Clearly seen is the decreasing streamwise correlation distance as *n* increases. Also apparent is that the *n*=0.4 case is not fully developed. The unsteadiness is comprised of just a few discrete "puff"-like structures. Consequently we do not expect results from its analysis to be entirely consistent with the other *n*.

The time-mean normalised velocity profiles in physical coordinates show only quite small differences (not shown), but plotted in wall coordinates reveal a consistent trend with flow index (see Figure 3). The near wall behaviour for all *n* is almost identical, with a linear viscous sub-layer extending to $y^+ \approx 10$. Such a layer is anticipated in the analyses in [2], [3].

As the flow becomes more shear-thinning (*n* decreasing from unity), the profiles for the power law fluids deviate from, and lie above, the Newtonian profile. For increasing shear-thickening (*n* increasing from unity) they deviate below the Newtonian curve. With the exception of *n*=0.4, these results also suggest the existence of a log-layer whose slope increases with decreasing flow index below unity, but with a slope that is approximately constant at 2.65 for $n \geq 1$. There is no obvious logarithmic region in the case of $n = 0.4$. These profiles are suggestive of less well-developed turbulence for more shear thinning flows ($n < 1$), and more well developed for shear thickening ($n > 1$).

The time-mean viscosity profiles (normalized by mean wall viscosity) are shown in Figure 4. As expected, mean centreline viscosities increase as *n* decreases and vice versa. In wall coordinates it is clear that the mean viscosity for all simulations does not begin to deviate from the wall value until towards the edge of the viscous sub-layer at around $y^+ \approx 6$, hence a linear velocity profile for the near wall layer is expected on this basis.

At the edge of the viscous sub-layer ($y^+ \approx 10$), the range of viscosity values for these flow indices is approximately ±50% of the wall value. Viscosity then rapidly deviates from the wall

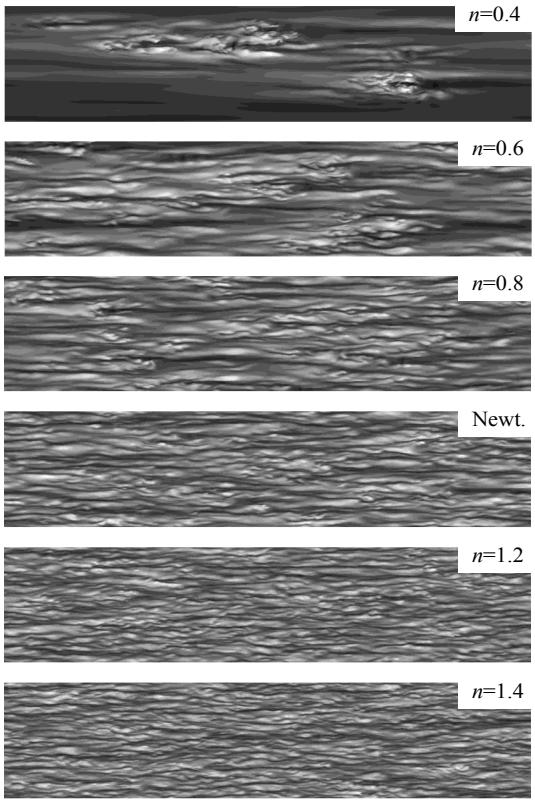

Figure 2 Instantaneous near-wall streamwise velocity contours on developed cylindrical surfaces obtained in preliminary calculations computed at a common domain length of $4\pi D$.

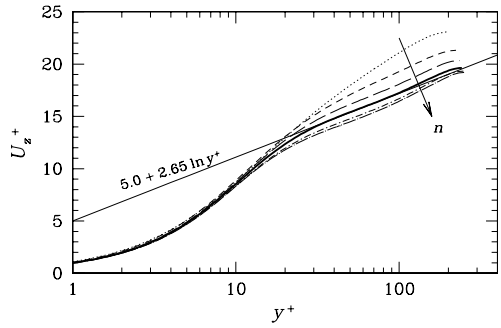

Figure 3 Mean axial velocity profile in wall coordinates. Profiles for $n < 1$ fall above the Newtonian curve $n > 1$ fall below.

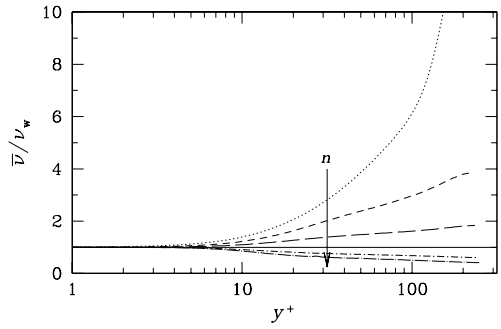

Figure 4 Mean normalised viscosity profile in wall coordinates. Note the wall viscosity is identical for each case by definition.

value in the log layer and core flow. In log wall coordinates, the viscosity increases/decreases almost linearly outside the viscous sub-layer, indicating a power law relationship between viscosity and distance from the wall for $n > 0.4$. There is no obvious functional relationship between the slope of the profile and the flow index that we have been able to determine.

Turbulence intensities

Turbulence intensities and Reynolds stress are not presented but follow similar trends to those reported in [9], with all (except axial turbulence intensity) decreasing as the flow index decreases. This decrease in turbulence intensity is expected on the basis of the increase in mean viscosity — higher viscosity will provide additional dissipation in shear thinning fluids, resulting in larger, weaker streamwise vortices. The slight increase in axial intensity compared to a Newtonian fluid has been observed in earlier work on shear thinning fluid [9], [10] as well as in visco-elastic fluids, e.g. [1] [5].

Turbulence kinetic energy

Space constraints limit the detail we can present, but some of the turbulence energy balance terms are plotted in Figure 5. For $n < 1$ the turbulent kinetic energy (q) is higher in the linear, buffer and lower log-layers (and vice versa for $n > 1$) although the q-curves cross over the Newtonian curve at $y^+ = 80$ depending on the exact value of n. The mean-flow turbulent production (term 10) is lower for $n < 1$ and occurs slightly further from the wall. The mean viscous transport (MVT, term 4) does not vary much with n except very near the wall ($y^+ < 3$), where it increases for $n < 1$. Because the mean viscosity is almost constant near the wall has the same value for all n, only the radial gradients of $\overline{s'_{rz}u'_z}$ contribute to MVT and increased values here reflect higher values of axial turbulence intensity, higher turbulent rate of strain and/or their closer correlation. The mean viscous dissipation (MVD, term 7) increases for $n < 1$, especially in the linear region where its magnitude is 50% greater for n =0.6 than the Newtonian case. Because the mean viscosity in the linear region is almost uniform in the viscous sub layer (and essentially independent of n), this means that the turbulent rate of strain tensor is larger here for $n < 1$, *i.e.* the fluctuating velocity gradients are higher.

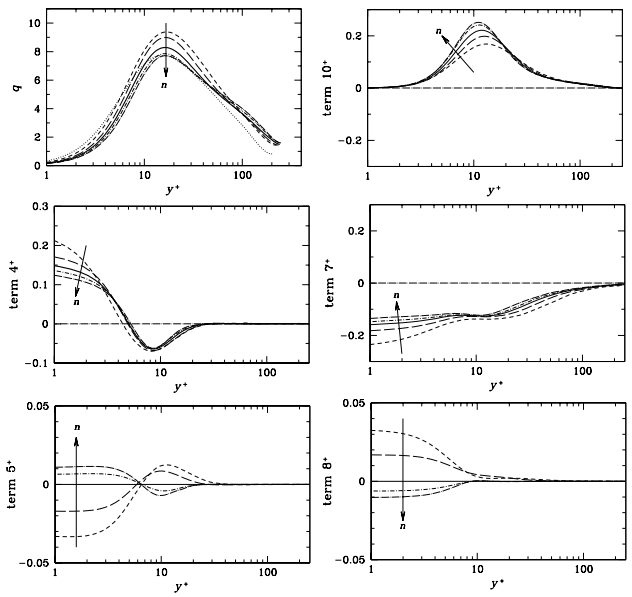

Figure 5 Turbulent kinetic energy (top left), production (term 10, top right), mean viscous transport (term 4, middle left), mean viscosity dissipation (term 7, middle right), mean shear turbulent viscous transport (MSVT) (term 5, bottom left) and turbulent shear stress–mean strain contraction (term 8, TSMS) (bottom right).

Of the four terms that do not appear in the Newtonian energy balance (MSVT, TVT, TSMS, TVD) only two of them make a significant contribution to the energy balance. The mean shear turbulent viscous transport (MSVT, term 5) is more negative for $n < 1$ in the viscous sub layer, changing to be positive at around $y^+ \approx 6$. Because the mean wall strain rate S_{rz} has a lower magnitude (and has negative sign) the viscosity-velocity correlation $\overline{\nu' u'_z}$ increases more rapidly away from the wall for $n < 1$. The turbulent shear stress-mean strain contraction (TSMS, term 8) follows the opposite trend of MSVT near the wall with higher values for $n < 1$, indicating a higher correlation $\overline{\nu' s'_{rz}}$. The sum of the two major non-Newtonian contributions (not shown) is non-zero and provides an additional source of turbulent kinetic energy for $n < 1$ (and sink for $n > 1$) with a peak near the edge of the sub-layer.

Conclusions

These preliminary results show that although there are differences between the turbulence profiles in power law and Newtonian fluids, shear thinning (or thickening) rheology does not effect major changes to the nature of the flow at a generalised Reynolds number of 7500. Shear thinning tends to damp turbulence velocity correlations except for the axial turbulence intensity. There is reduced turbulence production as n decreases. The results suggest that the turbulence kinetic energy budget is modified primarily by the mean shear turbulent viscous transport that is negative in the viscous sub-layer (damping turbulence energy) and the turbulent shear stress-mean strain contraction that is a source there.

Acknowledgments

We thank J.M.J. den Toonder for supplying experimental data and J.G.M. Eggels for copies of his PhD thesis. Computations were performed at the Australian Partnership for Advanced Computing National Facility, and we thank staff for their help.

References

[1] Beris, A. N. & Dimitropoulos, C. D. 1999 'Pseudospectral simulation of turbulent viscoelastic channel flow', *Comp. Meth. Appl. Mech. & Engng* **180**, 365–392.

[2] Clapp, R. M. 1961 'Turbulent heat transfer in pseudoplastic non-Newtonian fluids', *Int. Dev. Heat Mass Trans*. **III**, 652–661.

[3] Dodge, D. W. & Metzner, A. B. 1959 'Turbulent flow of non-Newtonian systems.' *A. I.Ch. E. J*. **5**, 189–204.

[4] Eggels, J. G., Unger, F., Wiess, M. H., Westerweel, J., Adrian, R. J., Friedrich, R. & Nieuwstadt, F. T. M. 1994 'Fully developed turbulent pipe flow: A comparison between direct numerical simulation and experiment'. *J. Fluid Mech.* **268**, 175–209.

[5] Escudier, M. P., Presti, F. & Smith, S. 1999 'Drag reduction in the turbulent pipe flow of polymers', *J. Non-Newt. Fluid Mech*. **81**, 197–213.

[6] Nguyen, Q. D. & Boger, D. V. 1998 'Application of rheology to solving tailings disposal problems', *Intnl J. Mineral Proc*. **54**, 217–233.

[7] Pinho, F. T. 2003 'A GNF framework for turbulent flow models of drag-reducing fluids and a proposal for a k-ε type closure', *J. Non-Newt. Fluid Mech*. **114**, 149–184.

[8] Piomelli, U. 1997 'Large-eddy simulations: Where we stand', *In Advances in DNS/LES* (ed. C. Liu & Z. Liu), pp. 93–104. AFOSR, Louisiana.

[9] Rudman, M., Blackburn, H. M., Graham, L. J. W. & Pullum, L. 2004 'Turbulent pipe flow of non-Newtonian fluids', *J. Non-Newt. Fluid Mech.* **118** (1), 33–48.

[10] Rudman, M. & Blackburn, H. M. 2006 'Direct numerical simulation of turbulent non-Newtonian flow using a spectral element method', *Appl. Math. Mod*. **30**, 1229–1248.

[11] den Toonder, J. M. J. & Nieuwstadt, F. T. M. 1997 'Reynolds number effects in a turbulent pipe flow for low to moderate Re', *Phys. Fluids* **9** (11), 3398–3409